Realistic Vendor-Specific Synthetic Ultrasound Data for Quality Assurance of 2-D Speckle Tracking Echocardiography: Simulation Pipeline and Open Access Database

Martino Alessandrini, Bidisha Chakraborty, Brecht Heyde, Olivier Bernard, Mathieu De Craene, Maxime Sermesant, and Jan D'hooge, *Member, IEEE*

***Abstract*— Two-dimensional (2-D) echocardiography is the modality of choice in the clinic for the diagnosis of cardiac disease. Hereto, speckle tracking (ST) packages complement visual assessment by the cardiologist by providing quantitative diagnostic markers of global and regional cardiac function (e.g., displacement, strain, and strain-rate). Yet, the reported high vendor-dependence between the outputs of different ST packages raises clinical concern and hampers the widespread dissemination of the ST technology. In part, this is due to the lack of a solid commonly accepted quality assurance pipeline for ST packages. Recently, we have developed a framework to benchmark ST algorithms for 3-D echocardiography by using realistic simulated volumetric echocardiographic recordings. Yet, 3-D echocardiography remains an emerging technology, whereas the compelling clinical concern is, so far, directed to the standardization of 2-D ST only. Therefore, by building upon our previous work, we present in this paper a pipeline to generate realistic synthetic sequences for 2-D ST algorithms. Hereto, the synthetic cardiac motion is obtained from a complex electromechanical heart model, whereas realistic vendor-specific texture is obtained by sampling a real clinical ultrasound recording. By modifying the parameters in our pipeline, we generated an open-access library of 105 synthetic sequences encompassing: 1) healthy and ischemic motion patterns; 2) the most common apical probe orientations; and 3) vendor-specific image quality from seven different systems. Ground truth deformation is also provided to allow performance analysis. The application of the provided data set is also demonstrated in the benchmarking of a recent academic ST algorithm.**

***Index Terms*— Database, echocardiography, elastic image registration, electromechanical modeling, ground truth, multivendor, open access, simulations, speckle tracking, standardization, validation.**

Manuscript received August 23, 2017; accepted December 17, 2017. Date of publication December 22, 2017; date of current version March 1, 2018. The work of M. Alessandrini was supported by the European Union's Horizon 2020 Research and Innovation Programme under the Marie Sklodowska-Curie Grant agreement 659082. *(Corresponding author: Martino Alessandrini.)*

M. Alessandrini was with the Laboratory on Cardiovascular Imaging and Dynamics, KU Leuven, 3000 Leuven, Belgium. He is now with the Department of Electrical, Electronic and Information Engineering, University of Bologna, 40127 Bologna, Italy (e-mail: martino.alessandrini@gmail.com).

B. Chakraborty, B. Heyde, and J. D'hooge are with the Laboratory on Cardiovascular Imaging and Dynamics, KU Leuven, 3000 Leuven, Belgium.

O. Bernard is with the Université de Lyon; CREATIS; CNRS UMR5220; Inserm U1044; INSA-Lyon; Université Lyon 1; 69622 Lyon, France.

M. De Craene is with Philips Research, 92156 Suresnes, France.

M. Sermesant is with the Inria-Asclepios Project, BP 93 06902 Sophia Antipolis, France.

Digital Object Identifier 10.1109/TUFFC.2017.2786300

I. Introduction

SPECKLE tracking echocardiography (STE) is available clinically to image cardiac displacement and strain noninvasively at an adequate temporal resolution. Clinical feasibility of STE derived strain has been shown in many studies: strain has been used to diagnose myocardial ischaemia; it has been proposed as a tool to predict infarct size after coronary reperfusion; it is recommended as routine measurement in patients undergoing chemotherapy; it has been proposed as a predictor of risk of ventricular arrhythmias; it may be applied to guide the placement of the pacing lead in patients receiving cardiac resynchronization therapy amongst others [1]. Strain is more sensitive than ejection fraction as a measure of systolic function [1] and has better prognostic value [2].

Yet, the compelling added diagnostic value is tempered by a major clinical concern connected to the reported poor reproducibility between the solutions provided by different vendors [3]. Such disagreement is not only due to obvious differences in accuracy coming from different technical implementations but also due to a lack of consensus on the definitions of the quantities of interest: Lagrangian versus Eulerian strain; endocardial versus midwall; end systolic versus peak systolic; definition of average values; definitions of the segments; and so on. Unfortunately, these sources of inconsistency are not easily accessible, since the underlying technical choices are not disclosed. Overall, this still holds back a more widespread dissemination of the STE technology. To address this issue, the European Association of Cardiovascular Imaging (EACVI) and the American Society of Echocardiography (ASE) along with representatives from all vendors have been endorsing a concerted effort (a "task force") aimed at reducing intervendor variability of strain measurements [4].

Importantly, part of this effort has resulted in a first consensus document providing definitions and procedures to compute global and segmental longitudinal strain [5]. A further activity consisted in the quantification of intervendor differences through head-to-head comparison studies both *in vivo* [6] and *in silico* [7]. Unlike an *in vivo* setup, an *in silico* evaluation makes it possible to assess the absolute accuracy of a method in a fully controllable and reproducible setting [7]. In a first

study, a synthetic data set was therefore used to benchmark global longitudinal strain (GLS) measurements of nine different vendors of STE packages [7].

Synthetic sequences used in [7] were based on a kinematic model of cardiac contraction while a binary rule was used to assign ultrasound speckle texture, i.e., bright speckle inside the myocardium and darker speckle elsewhere. The parametric motion model allowed modifying global motion descriptors and therefore to evaluate GLS sensitivity while the relative contrast between myocardium and surrounding regions could be adjusted to measure robustness to noise [7].

Despite the important insights provided in [7], such a simple simulation setup faced intrinsic limitations. On the one side, the simple speckle model could oversimplify, and therefore bias, the tracking problem. On the other, the global motion model could not be used to alter, and therefore benchmark, regional function [7]. There is thus a compelling need for more representative ground truth data for STE algorithms.

Recently, we have described a pipeline to simulate realistic ground truth sequences for 3-D STE algorithms [8]. The pipeline used a complex electromechanical heart model to compute realistic physiological and pathological motion patterns which could account for regional dysfunction [9]. Moreover, the simulated 3-D sequences were visually similar to real recordings thanks to a strategy that allowed sampling the synthetic speckle texture from a real volumetric recording. The pipeline in [8] was recently used to benchmark several 3-D speckle tracking (ST) algorithms from academia [10]. Recently, that framework was extended to the simulation of cine and tagged magnetic resonance data sets [11].

Yet, 3-D echocardiography is still an emerging technology in the clinic and therefore the priority, as embodied by the EACVI/ASE/Industry task force, is so far directed to 2-D echocardiography only [5], [7]. Unfortunately, the pipeline in [8] cannot be used directly to simulate reliable 2-D ground truth sequences. Indeed, simple slicing of the simulated 3-D volumes obtained with [8] would not produce representative 2-D simulations, since: 1) the field of view in 2-D is typically wider and 2) the image quality (i.e., spatial resolution) is typically higher. Therefore, we describe here a new framework to simulate representative 2-D ground truth synthetic sequences for 2-D STE algorithms.

As in [8] and [10], the ultrasound images are simulated from a cloud of point scatterers. To have realistic speckle texture, scattering amplitude is sampled from a real clinical recording working as a "template." An electromechanical (E/M) cardiac model is then used to displace the scatterers inside the myocardium and therefore to have a realistic heart motion in the simulated image sequences. Yet, unlike in [8], in order to obtain realistic 2-D simulated images, we employ 2-D clinical recordings as templates. This implies solving the consequent 2-D/3-D spatio-temporal registration problem between the 2-D template and the 3-D ground truth motion given by the electromechanical model instead of a 3-D/3-D registration problem as in [8]. Furthermore, we include a strategy to mitigate the existing border artifacts visible in [8] at the interface between the myocardium and the blood pool. These are dealt with by implementing a smooth transition between the speckle properties in the two regions. Of note, such border artifacts were often identified as a source of poor realism in [8]. In addition, most importantly in our context, border artifacts could bias the initial segmentation step of an STE algorithm. Finally, unlike [8], the new 2-D pipeline sets a prescribed density of incoherent scatterers in the myocardium. This overcomes a further limitation of [8], where speckle coherency was found to be unrealistically high. High temporal coherency could also bias the tracking problem. As in [8], the ultrasound images were simulated from the scatter maps by using the fast ultrasound simulator named "COLE" [12].

By changing the ground truth motion model, the adopted template recording, and the probe settings in the ultrasound simulator, the new pipeline is used to generate a diverse set of 105 ground truth sequences encompassing: 1) healthy and ischemic motion patterns; 2) the most common apical probe orientations (i.e., two chambers, three chambers, and four chambers); and 3) vendor-specific image quality from seven systems. This last aspect in particular was the result of a concerted effort together with some representatives from the vendors involved who engaged to provide high-quality template sequences for our study and to disclose some details of the acquisition setup to be used in the ultrasound simulator [12]. The data set can therefore be used to benchmark sensitivity to changing global and regional function as well as changing image appearance between vendors. This data set is made available to the research community at our project Web page (see Section IV-A).

A preliminary version of this paper was presented in the proceeding paper [13], which is extended in several ways. At first, the database presented here is larger (105 sequences versus four sequences in [13]) and more diverse in terms of probe orientation (two-, three-, and four-chamber views versus two and four chambers in [13]) and motion pattern (5 kinds of ischemia versus 2 in [13]). Moreover, unlike [13], we include vendor specific speckle texture from seven different vendors. Finally, none of the techniques presented here to solve the simulation artifacts were present in [13]. In addition, we show the feasibility of the provided synthetic data set by using it in the evaluation of one technique developed recently in our group [14].

This paper proceeds as follows. In Section II, we describe the simulation pipeline. In Section III, we define the ground truth quantities derived from the synthetic data and present the evaluation of the considered ST technique. Section IV describes the simulated data set and the evaluation result. Section V follows with the discussion whereas this paper is concluded in Section VI.

II. Simulation Pipeline

The flowchart of the proposed simulation pipeline is provided in Fig. 1. Each block contains a reference to the corresponding section in this paper where its content is described. Real ultrasound recordings are used to transfer realistic texture to the simulated sequences (block 1). The first step in the simulation pipeline is to align a detailed biventricular 3-D anatomy (block 2) to the 2-D template recording. The result

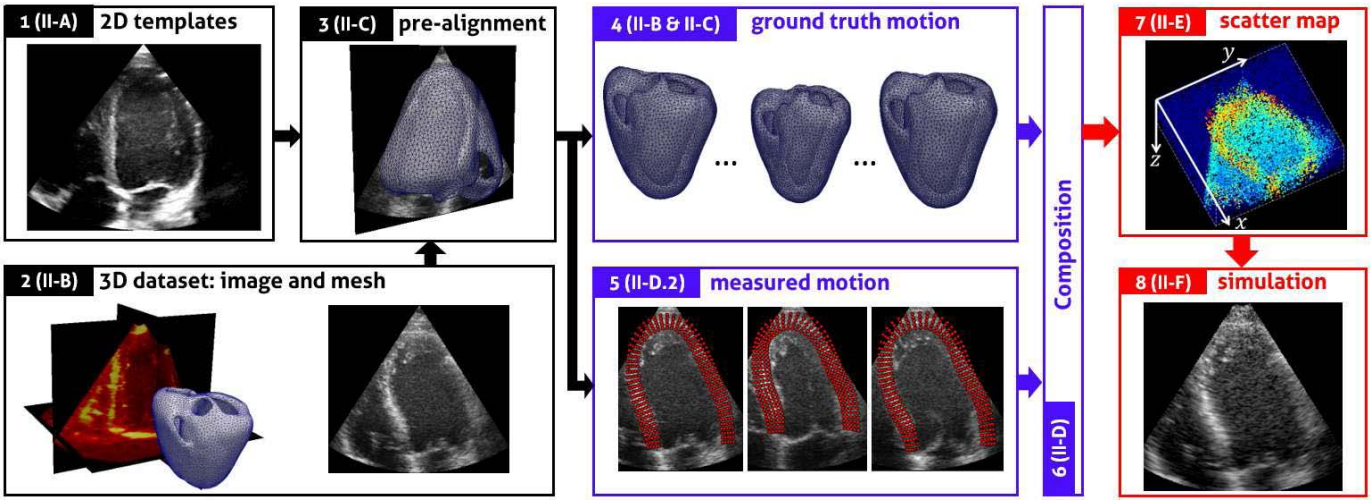

Fig. 1. Flowchart of the proposed simulation pipeline. Each block reports within brackets the corresponding section describing its content. The black part contains the necessary preprocessing to align the 2-D template with the 3-D mesh. The blue part contains the computation of the synthetic displacement field (i.e., the ground truth). The red part contains the ultrasound simulation. Please refer to the main text for a detailed description.

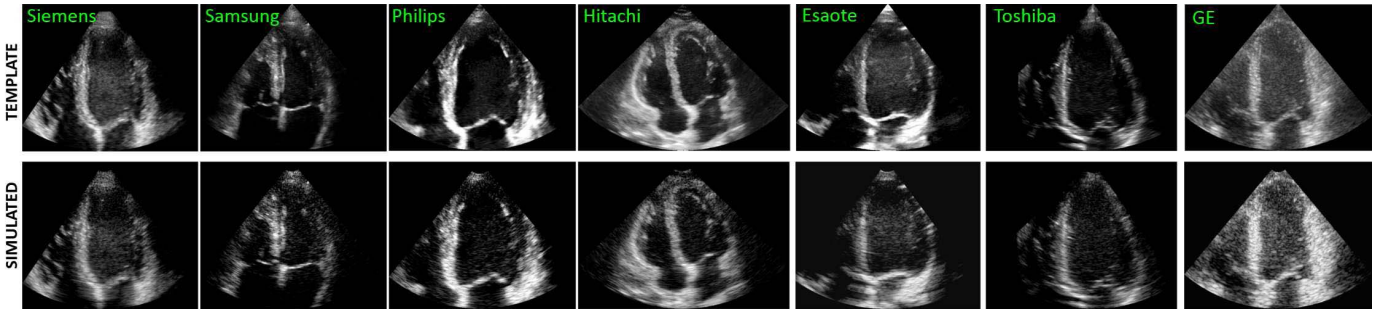

Fig. 2. Sample template sequences (4-ch, end diastolic frame) from the seven vendors (first row) and corresponding simulated images (second row).

is displayed in block 3. The electromechanical simulator is run on the 3-D anatomy to generate the ground truth motion field for one cardiac cycle (block 4). In order to apply the ground truth motion field to the 2-D template, the cardiac motion in the template recording has to be computed (block 5) and compensated for (block 6). The ground truth motion is then used to displace a cloud of point scatterers (block 7). Thanks to the composition between the ground truth and the computed motion field, scattering amplitude can be sampled from the template recording. The ultrasound simulator is then run on the scatter map to generate the synthetic images (block 8). The simulated sequence will look like the template recording but cardiac motion will be fully determined by the electromechanical simulation and, hence, available for benchmarking. A detailed description of the pipeline follows.

A. Template Recordings

For each vendor involved, we used one apical four-chamber (4-ch), one apical three-chamber (3-ch), and one apical two-chamber (2-ch) cine recording as a template for the subsequent simulation steps. One full cardiac cycle from end-of-diastole (ED) was retained from each recording. We included the seven manufacturers of ultrasound systems already involved in the EACVI/ASE/Industry standardization task force [6], [7]. The specific vendors and relative systems were therefore: General Electrics, GE (Vivid E9 version 112.1.3); Hitachi-Aloka (Prosound α7 CV version 6.1); Esaote (MyLab Alpha); Philips (iE 33 Vision 2012); Samsung (EK07); Siemens (SC2000 version 3.5); and Toshiba (Artida version 3.0).

The template recordings were retrieved from the database created in the context of the first intervendor study [6] and available at the University Hospital Gasthuisberg, KU Leuven, Leuven, Belgium. In this version of the data set, we were interested in generating, for each vendor, synthetic recordings with good visual quality. As explained later, this implies working with high-quality templates. Hereto, the selected sequences were then transmitted to the representatives of the relevant vendors for quality check. Whenever considered necessary, alternative, good quality sequences were sent back to us by the vendors. As such, 21 (7 vendors $\times$ 3 apical views) multivendor high-quality template recordings were available. Example frames are provided in Fig. 2 (first row). For all vendors but GE, templates were provided as dicom data exported from the respective systems, from which the image sector was extracted by using custom software written in MATLAB R2017a (The MathWorks, Inc., Natick, MA, USA). GE provided instead raw radio frequency (RF) signals along with the MATLAB scripts to reconstruct the images.

In addition, all vendors agreed to disclose some of the acquisition settings, such as temporal resolution, scan depth, focus depth, beam density, center frequency, and bandwidth. These

settings were used to make the simulated acquisition sequence as close as possible to the real systems (see Section II-F).

B. 3-D Geometry and Electromechanical Model

The E/M simulations used were the same as in [8]. Briefly, left and right ventricles (RVs) were segmented from a 3-D ultrasound recording (Philips iE33 ultrasound machine with an X5 matrix array transducer) by using proprietary model-based full heart segmentation software by Philips [see Fig. 4(a)]. The segmented volume was then converted into a tetrahedral mesh by using a MATLAB wrap of the Computational Geometry Algorithms Library[1] [15]. The segmented geometry was then animated by applying the Bestel–Clement–Sorine E/M model [9] as implemented in the Simulation Open Framework Architecture[2] [16] developed by Inria. By altering the model's contractility and stiffness, we simulated three kinds of segments: normal, mildly ischemic, and fully ischemic. Segments were defined as per the standard 17 segments model defined by the American Heart Association [17]. The three kinds of segments were combined to realize five motion patterns, one healthy and four ischemic ones corresponding to: a distal and proximal occlusion of the Left Anterior Descending artery (LADdist and LADprox, respectively); occlusions of Right Coronary Artery (RCA) and Left Circumflex (LCX). Please refer to [8] for more details.

As such, a series of tetrahedral meshes was available for each simulation to span one cardiac cycle starting from ED. Temporal resolution (i.e., the number of meshes) was adjusted for each vendor in order to match the frame rate of the specific system. Fig. 3 illustrates the three considered image planes and the mechanical properties of each segment in the four ischemic simulations. Of note, the RV was only used to have a balanced E/M simulation. Our focus being on left ventricular dynamics, the RV was therefore excluded from the meshes resulting from the E/M simulation. Hence, in the following, when referring to the 3-D model, we will be referring to the left ventricle (LV) only.

C. Initial Alignment of the 3-D Simulation and the 2-D Template

The first step was to align, for each vendor and each apical view, the 3-D simulation and the 2-D template at time 0, i.e., at ED. As mentioned, the 3-D geometry was obtained by segmenting a 3-D echocardiographic scan.

The procedure consisted of the following steps, as illustrated in Fig. 4.

1) From the 3-D echocardiographic scan used to construct the 3-D geometry, we extracted one 2-D slice corresponding to the specific apical view of the 2-D template. Hereto, we used a slicing plane containing the LV long axis and rotated 0°, 60°, or 90° depending on whether the 2-D template corresponded to a 4-ch, 3-ch, or 2-ch view, respectively. Angles are referred to a clockwise rotation looking from the LV apex to the LV base. The segmentation of the three extracted apical slices was directly available from the 3-D model [see Fig. 4(b) for the extracted 4-ch slice].
2) The LV myocardium was contoured manually on the first frame of the 2-D template. This contour was used to drive the alignment with the 3-D model, as described later. In order for this alignment to be correct, it was essential to have consistent contouring between the 2-D template and the sliced 3-D volume. In practice, this implied having a consistent definition of the cut levels at the LV base. To ensure consistency, the 2-D template was segmented by using the corresponding segmentation of the sliced 3-D volume as a visual reference. This process is illustrated in Fig. 4(c) for the 4-ch view from Toshiba: the LV myocardium was contoured manually

[1] http://www.cgal.org/
[2] https://www.sofa-framework.org/

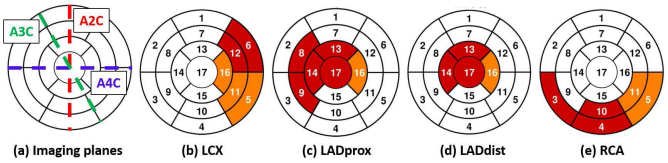

Fig. 3. (a) Bull's eye plots with imaging planes and an illustration of ischemic (red) and neighboring (orange) segments for (b) LCX, (c) LADprox, (d) LADdist, and (e) RCA mechanical simulations.

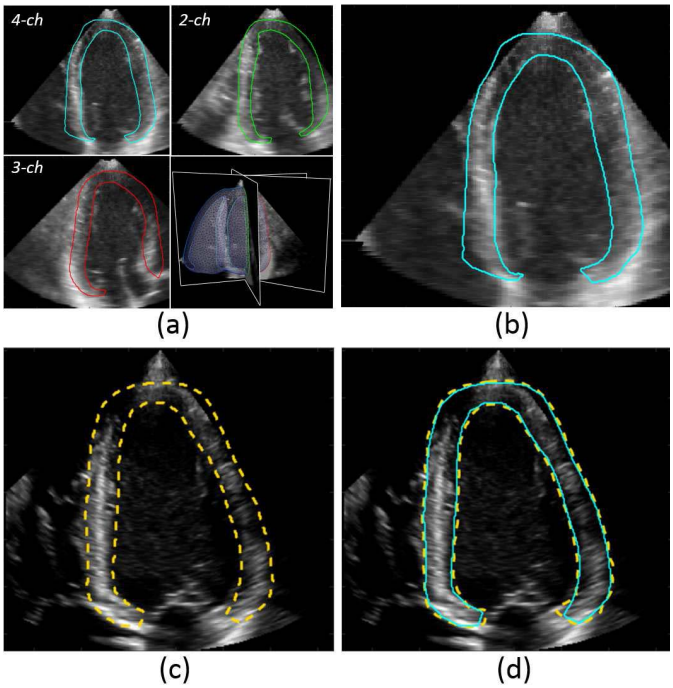

Fig. 4. Three apical views are sliced from both the 3-D image volume and the 3-D mesh by using fixed rotation angles around the LV long axis, as described in the text. (a) Three extracted image slices, the full 3-D anatomical model (i.e., the transparent tetrahedral mesh overlaid), as well as the intersections of the 3-D model with the sliced image planes: intersection with the 4-ch slice (cyan); intersection with the 2-ch slice (green); intersection with the 3-ch slice (red). (b) 4-ch slice along with the associated contour (cyan). (c) First frame of the 4-ch template recording from Toshiba along with the associated segmentation (the dashed orange contour), drawn manually in order to match the cyan contour in (b). (d) 3-D geometry is deformed in order to match the template frame. The final deformation aligns the green contour onto the orange one.

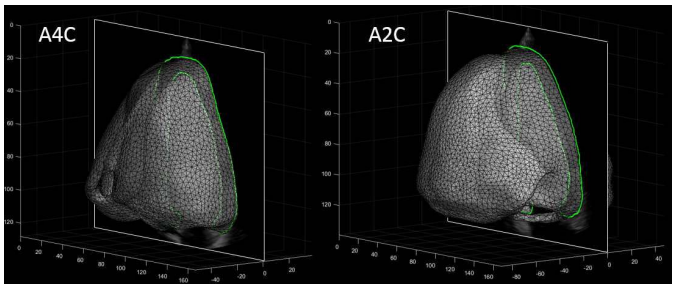

Fig. 5. Result of the 3-D/2-D registration step described in Section II-C. After registration, the 3-D biventricular model (i.e., the tetrahedral mesh in the figure) is aligned with the first frame of the 2-D template recording. The green contour represents the intersection between the 3-D model and the image plane. The result of the alignment is illustrated for an apical 4-ch (left) and an apical 2-ch (right) view from Toshiba.

(dashed orange contour) on the template by using the cyan contour in Fig. 4(b) as a visual reference.

3) The segmentation of the sliced 3-D geometry [cyan contour in Fig. 4(b)] was then registered onto the segmentation of the 2-D template [dashed orange contour in Fig. 4(c)]. Hereto, both contours were initially converted to binary masks and aligned by rigid registration. To refine the alignment, we used nonrigid free-form registration as implemented in the Medical Image Registration Toolbox, developed by Andriy Myronenko and available open source at https://sites.google.com/site/myronenko/research/mirt. Sum-of-squared-differences (SSD) was used as a dissimilarity metric and its computation was restricted in space to a mask surrounding the myocardium. The deformation field was parameterized with B-splines and regularization was enforced by Laplacian penalization of the displacements of the B-spline control points [18]. The parameters of the registration algorithm (i.e., grid spacing, number of pyramidal levels, and regularization weight) were tuned by optimizing visual matching. The final alignment of the two contours is illustrated in Fig. 4(d).
4) The transformation between slices, as computed in the previous step, was used to align the first of the 3-D geometries. Hereto, the 2-D transform, defined on the image plane, was used to displace the in-plane coordinates of the nodes of the 3-D mesh. As mentioned, this involved an initial rigid registration followed by a nonrigid refinement. To keep the 3-D deformed geometry balanced, the out of plane coordinate of the mesh nodes was scaled by using the same scaling factor found in the initial rigid registration step. This way, a possible change in size was distributed uniformly along the three dimensions. At the end of this step, the 2-D template and the 3-D geometry were aligned, as illustrated in Fig. 5 for the Toshiba template.
5) The same transform found for the first 3-D geometry was then applied to the full time series.

As such, for each vendor and each apical view, we obtained a specific set of tetrahedral meshes corresponding to one simulated heart beat and initially (i.e., at time 0) aligned with the 2-D image template. These meshes will define the ground truth values of deformation and strain for the specific template, as explained later in this paper. Section II-D will explain how to compute a spatio-temporal transform that extends the alignment between the 2-D template and the 3-D simulation to the full cardiac cycle. Such a transform will be fundamental to sample scatter amplitude from the template recording and therefore to obtain realistic simulated images. In the following, we will assume therefore that the 3-D geometries have been prealigned as described in this section.

D. Spatio-Temporal Alignment

1) Template Space and Simulation Space: Template and simulation have different dimensionalities. The template is defined on the image slice. A point in the template space is therefore $\mathbf{y} = [y_1, y_2] \in \Omega_{\text{im}}$, with $\Omega_{\text{im}} = w \times h$, being w and h image width and height. The simulation has an additional dimension perpendicular to the image plane. A point in the simulation space is therefore $\mathbf{x} = [x_1, x_2, x_3] \in \Omega_{\text{sim}}$, with $\Omega_{\text{sim}} = \Omega_{\text{im}} \times I_d$, being I_d a 1-D segment of length d centered on the image plane and perpendicular to it. This is also illustrated in Figs. 5 and 6. The thickness d of the 3-D slab was chosen empirically to prevent out-of-plane motion components in the E/M model from creating holes in the simulated images.

2) Motion Field in the Template: The goal is to find a displacement field in the template recording. Hereto, we used an elastic registration technique [14] to compute a set of temporally corresponding points sampling the myocardium uniformly over time. Thin plane splines (TPSs) [19] were then used to extrapolate cardiac motion from the discrete point set to the entire image space.

More formally, given the initial position of a point $\mathbf{y}$ at time 0, TPS find its matched position $\mathcal{F}(\mathbf{y}, t) = \mathbf{y} + \mathbf{f}(\mathbf{y}, t)$ at time t, being $\mathbf{f}(\cdot, t)$ the extrapolated displacement field at time t.

3) Extrapolating the Synthetic Cardiac Motion: In a similar manner, we used TPS to extrapolate cardiac motion to surrounding regions in the simulation space by using the nodes of the E/M meshes as control points. Specifically, given a point $\mathbf{x}$ at time 0, its position at time t is $\mathcal{G}(\mathbf{x}, t) = \mathbf{x} + \mathbf{g}(\mathbf{x}, t)$, being $\mathbf{g}(\cdot, t)$ the extrapolated displacement field at time t.

4) Temporal Matching: The goal is to synchronize template and simulation by aligning corresponding phases of the cardiac cycle. Namely, we seek for a mapping $t_T = t_T(t_S)$ between the time axis in the simulation (t_S) and the template recording (t_T). As in [8], we linearly stretch/compress the t_T axis in order to match a set of relevant cardiac events. Hereto, we used three cardiac events for matching: first ED (i.e., the first frame), end-of-systole (ES), and the second ED (i.e., the last frame). ES was identified visually on template and the simulation based on minimum volume of the LV chamber.

E. Scatter Map Generation

Each image frame was simulated from the combination of two scatter maps: one *coherent* scatter map and one *incoherent*

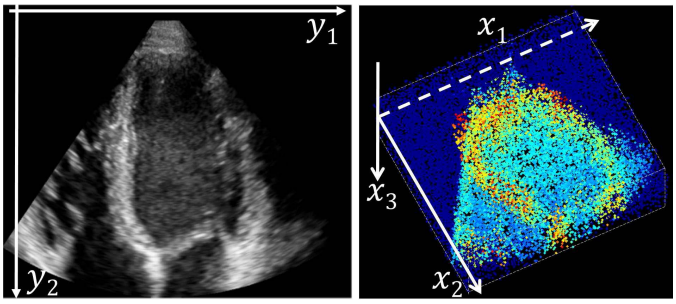

Fig. 6. Left: first frame of the 2-D template recording. y_1 and y_2 represent the coordinate axes in the image space. Right: scatter map corresponding to the first simulated frame. Color encodes scatter amplitude according to a "jet" color-map: blue means low amplitude and red means high amplitude. Scatter amplitude was sampled from the template frame on the left. x_1, x_2, and x_3 are the coordinate axes in simulation space. The through-plane coordinate x_3 was added to avoid the effect of out-of-plane motion components, as discussed in the main text.

scatter map. Both scatter maps evolved in time to account for cardiac motion. In both the cases, scatterers were distributed on Ω_{sim} by following a uniform random distribution. The total number of scatterers N_s was established experimentally in order to have realistic speckle statistics in the simulated images. This evaluation is presented in [8]. In total, we used 2 million scatterers for each scatter map.

1) Scatter Map on the First Frame: We generated N_s scatterers randomly in Ω_{sim}. The position of the ith scatterer is denoted as $\mathbf{x}_i = [x_1^i, x_2^i, x_3^i]$, with $i = 0, \ldots, N_s - 1$. The x_1 and x_2 coordinates belong to the image plane, whereas x_3 is the out-of-plane coordinate (i.e., the azimuth), as illustrated in Fig. 6.

2) Coherent Scatter Map: The coherent scatter map was computed by taking the scatterers generated on the first frame and propagating them over time by using $\mathbf{x}_i(t_S) = \mathcal{G}(\mathbf{x}_i(0), t_S)$. Temporal coherency is given by the fact that the same scatterer is followed over the full simulation.

3) Incoherent Scatter Map: At each simulation time t_S, we regenerated new random scatterers in the ED frame and moved them to their correct configuration by $\mathbf{x}_i(t_S) = \mathcal{G}(\mathbf{x}_i, t_S)$. Therefore, unlike the coherent scatter map, there was no correspondence between scatterers at different simulation times in the incoherent scatter map.

4) Final Scatter Map: The final scatter map was obtained by mixing, at each simulation time, the coherent and incoherent scatter maps. Conceptually, coherent scatterers were mainly placed in the myocardium to enable ST, while incoherent scatterers were mainly placed in the background to account for the typical lack of speckle coherency in the blood. In our previous work [8], [13], the assignment was made based on a binary rule: coherent scatterers only in the myocardium and incoherent scatterers only in the background. This abrupt transition was sometimes the origin of mild artifacts at the interface between the two regions. To remove this effect, we applied here a smoother transition. This was implemented by using a smooth mask, as illustrated in Fig. 7(a), which, for each position, defines the probability of accepting a coherent scatterer and rejecting an incoherent one. The probability map was obtained by decreasing linearly from a value $p = 0.9$ inside the myocardium to a value $p = 0$, with a transition zone of 15 mm. The width of the transition zone was tuned visually in order maximize the realism of the simulations. Of note, we allowed a 10% of incoherent component inside the myocardium. The presence of incoherent speckle inside the myocardium is observed experimentally.

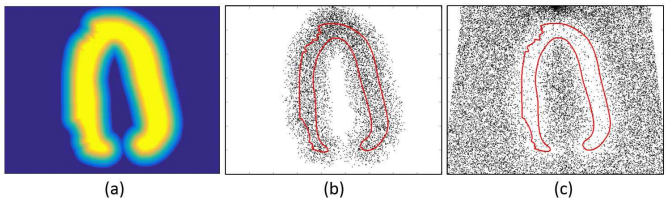

Fig. 7. (a) Probability map used to mix coherent and incoherent scatter maps. (b) Selected coherent scatterers. (c) Selected incoherent scatterers. The red contour in (b) and (c) denotes the myocardial mask. Note that we allow both incoherent scatterers inside the myocardium and coherent scatterers in the background. The scatter map was subsampled for readability of the figure.

To apply the acceptance/rejection rule, we assigned each scatterer a number w_i, picked randomly in the interval $[0, 1]$. Therefore, we accepted a coherent scatterer $\mathbf{x}_i$ if $w_i < p(\mathbf{x}_i)$; otherwise we rejected it. Similarly, we accepted an incoherent scatter if $w_i > p(\mathbf{x}_i)$. The set of selected coherent and incoherent scatterers is illustrated in Fig. 7.

Of note, this is different from what done in [11], where a smoothing mask was used to weight scattering amplitude between myocardium and surrounding structures. By that, speckle coherency in the myocardium was expected to remain high as in [8]. High speckle coherency was identified as a source of poor realism in [8] and could oversimplify the ST problem.

5) Scattering Amplitude: The amplitude a_i of myocardial scatterers (i.e., belonging to the region enclosed by the E/M meshes) was sampled from the first frame of the template recording and kept constant over time, i.e., $a_i(t_S) = a_i(0) = I(\mathbf{y}_i, 0)$, where $\mathbf{y}_i = [x_1^i, x_2^i]$ and $I(\cdot, k)$ denote the kth template frame. This choice was made to enforce speckle coherency inside the myocardium. The amplitude of background scatterers was instead sampled from the matched frame in the template recording, i.e., $a_i(t_S) = I(\mathcal{F}(\mathbf{y}_i, t_T), t_T)$. This strategy allowed having realistic moving texture for surrounding structures. Moreover, as in [8], to compensate for the logarithmic compression performed by ultrasound systems before display, we applied a mapping $\hat{a}_i = F(a_i)$ such that $20\log_{10}[F(a_i)] + \text{dB} = \text{dB} \cdot (a_i/255)$, where dB is the desired contrast in decibel in the simulated image. We have assumed a common 8-bit representation for template recordings.

F. Ultrasound Simulation

The ultrasound simulations were performed with the in-house COLE simulator [12]. We used the 3-D scatter maps to simulate 2-D images corresponding to azimuth $x_3 = 0$. Synthetic probe settings (scan depth, focus depth, field of view, beam density, center frequency, sampling frequency, and bandwidth) were specialized by using the values communicated by each vendor upon signature of nondisclosure agreements. Simulated RF lines were envelope detected, log compressed, and scan converted to obtain B-mode voxel images. Scan

converted images were resampled to match the pixel size of the corresponding template. Image reconstruction was therefore performed using our in-house algorithms which may differ from the company reconstruction algorithms. This in itself could have impact on the appearance of the resulting images (see Fig. 2).

As such, we generated a data set of 105 ground truth sequences (7 vendors $\times 3$ apical views $\times 5$ motion patterns.).

III. Evaluation

A. Ground Truth

We defined ground truth displacement and strain in agreement with the recent recommendations from the EACVI/ASE/Industry task force [5]. Hereto, we defined a set of seed points sampling the LV myocardium regularly along the longitudinal (36 points) and radial (5 points) directions. Longitudinal sampling was parameterized by the arc-length as computed with spline interpolation. The radial direction was computed as being normal to the longitudinal one. The five radial points were distributed uniformly between endocardium and epicardium. Endocardial and epicardial masks were defined manually on the first frame of each simulated recording. Points were further subdivided into six segments (in clockwise order: left-base, left-middle, left-apical, right-apical, right-middle, and right basal), obtained by splitting the endocardial contour into six parts with the same arc-length.

The seed points were anchored to the E/M by keeping barycentric coordinates constant over time. To account for the fact that the E/M model might produce out-of-plane motion components, we constantly reproject the seed point on the image plane at each frame. As such, a 2-D cloud of corresponding points was available for the full simulated cine-loop. We call these points $\mathbf{p}^i_{k_l,k_r}$, where $k_l = 0, \ldots, N_l - 1$ indicates the longitudinal coordinate, $k_r = 0, \ldots, N_r - 1$ indicates the radial coordinate, and $i = 0, \ldots, N_{\text{sim}} - 1$ is the time frame. $N_l = 36$ is the number of longitudinal points, $N_r = 5$ is the number of radial points, and N_{sim} is the (vendor dependent) number of simulated frames.

The time series of seed points were used to define the ground truth strain values. By using Lagrangian formulation [5], longitudinal (L-) strain at simulation time i was computed as $\epsilon^i_L = (L^i - L^0)/L^0$, where L^i is either the length of a segment (segmental strain) or the length of the LV contour (GLS). Arc-length was computed by using a continuous interpolation by cubic splines. Namely, cubic spline interpolation was used to obtain a parametric function $\mathbf{p}^i_{k_r}(l)$ in the continuous longitudinal variable $l \in [0, L^i_{k_r}]$, being $L^i_{k_r}$ the length of the full arc at transmural layer k_r measured by accumulating Euclidean distances, i.e., $L^i_{k_r} = \sum_{k_l=0}^{N_l-2} \|\mathbf{p}^i_{k_l+1,k_r} - \mathbf{p}^i_{k_l,k_r}\|$. Arc-length was then computed by numerical integration

$$L(l_a, l_b)^i = \int_{l_a}^{l_b} \left\| \frac{d\mathbf{p}^i_{k_r}(l)}{dl} \right\| dl. \tag{1}$$

Segmental and global strain were computed by setting the integration interval appropriately (for longitudinal strain, $l_a = 0$ and $l_b = L^i_{k_r}$). L-strain could be evaluated at five trans-mural layers. Radial (R-) strain was defined similarly by considering the relative change in distance between points in the radial direction. Segmental and global (GRS) R-strain were computed by averaging local estimates. Strain drift was compensated for retrospectively by distributing it linearly over the full cardiac cycle.

B. Considered Speckle Tracking Algorithm

To illustrate that the generated sequences are suited for ST, we used them to evaluate one recent ST technique developed in our laboratory [20]. The technique is based on elastic registration and uses a B-splice parametrization of the displacement field. The displacement is retrieved by minimizing an energy function expressed as the sum of a data term and a penalty. SSD between the intensity of the two registered frames was used as a data term and bending energy was used as a penalty.

The algorithm returned a dense displacement field $\mathbf{d}_{i\to i+1}(\mathbf{x})$ between pairs of subsequent frames $I_i(\mathbf{x})$ and $I_{i+1}(\mathbf{x})$. The computed displacement field was used to propagate the ground-truth seed points $\mathbf{p}^0_{k_l,k_r}$ available on the first frame through the entire cardiac cycle. Namely, a new set of points $\tilde{\mathbf{p}}^i_{k_l,k_r}$ was incrementally computed as $\tilde{\mathbf{p}}^i_{k_l,k_r} = \tilde{\mathbf{p}}^{i-1}_{k_l,k_r} + \mathbf{d}_{i-1\to i}(\tilde{\mathbf{p}}^{i-1}_{k_l,k_r})$ for $i = 1, \ldots, N_{sim-1}$ and $\tilde{\mathbf{p}}^0_{k_l,k_r} = \mathbf{p}^0_{k_l,k_r}$ for $i = 0$. As such, for each simulated sequence, we had the trajectory estimated by the ST algorithm $\tilde{\mathbf{p}}$ and the real trajectory $\mathbf{p}$ given by the ground truth. Tracking accuracy was then measured by comparing the two. The computed set of points $\tilde{\mathbf{p}}$ were used to compute segmental and global strain as described before and compared against the ground truth. Hereto, the slope (α) of the regression line between the estimate and the ground truth, the regression coefficient (ρ), bias (μ), and limits of agreement (LOA $= 1.96\sigma$) were considered as performance indexes. Furthermore, we tested the classification accuracy when using the computed strain values to detect ischemia by measuring the area under the curve (AUC) of the receiver operating characteristic (ROC) curves. The ROC curves were computed from a progressive threshold by assuming ES (absolute) strain values below the threshold as indicative of ischemia.

Fisher's transformation was used to test the hypothesis of no correlation. Strain bias was instead evaluated with a t-test. The statistical significance of the reported AUC values (i.e., of AUC > 0.5) was tested with the nonparametric technique described in [21].

The algorithm was tuned to maximize tracking accuracy on the healthy simulated GE sequences and tested on the remaining data. The most sensitive parameters in the evaluated algorithm were the weight put on the penalty term and the spacing between the B-spline knots. Both parameters impact the smoothness of the retrieved deformation field and the sensitivity to small deformations.

IV. Results

A. Open Access Database

Example images simulated with the proposed pipeline for the seven vendors are given in Fig. 2. Please note the

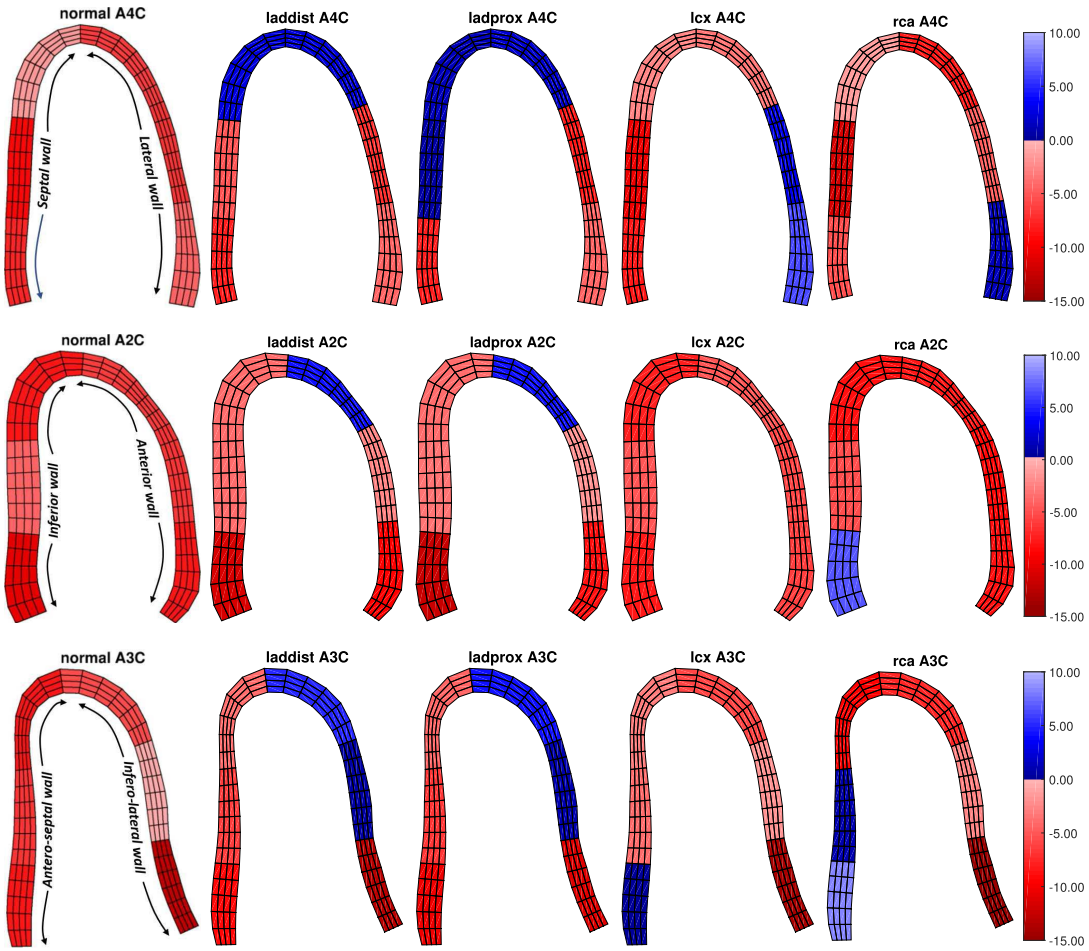

Fig. 8. Each image represents the LV myocardium in a 4-ch (top row), 2-ch (middle row), and 3-ch (bottom row) view. The quadrangular meshes, represented as wire-frames, were obtained by taking the 36×5 ground-truth seed points as nodes. Columns correspond to different motion patterns (the healthy simulation in the first column and the four ischemic ones in the remaining columns). Segments are colored according to the average ground truth L-strain value over all vendors. Note that impaired segments are in agreement with Fig. 3.

resemblance with the corresponding templates. Also, we stress that image reconstruction from the simulated RF signals was done with our in-house algorithm which may in general differ from the ones by the specific vendors. This might have an effect on the appearance of the simulated images.

The open database of 105 sequences can be accessed either from our departmental Web page[3] or directly at http://bit.ly/SyntheticDataQA2-DSTE. The database includes pixel images, the scatter maps, the ground truth seed points, and the MATLAB scripts to compute ground truth values of global and segmental L- and R- strain. Simulated RF data cannot be distributed directly, since they could enable reverse-engineering of the probe settings, which have been covered by nondisclosure agreements. Yet, synthetic RF data for arbitrary probe settings can be easily generated by a user from the provided scatter maps.

B. Mechanical Properties of the Synthetic Data Set

Maps of segmental end systolic L-strain are presented in Fig. 8. Segments were colored according to the average values over all seven vendors, which were not necessarily equal due to the registration step in Section II-C. Note that impaired segments are in full agreement with Fig. 3. Simulated ischemia, therefore, effectively reduces regional LV function in the expected perfusion territories. Yet, values of L-strain for normal cases remain below the reported normality ranges. This point will be discussed further in Section.

C. Evaluation of the Speckle Tracking Algorithm

The performance indexes for ES L-strain are reported in Table I. Strain accuracy varies between vendors due to the different image appearances. Fig. 9 displays the correlation plots for the seven vendors. Healthy and ischemic segments, defined according to Fig. 3, are colored in green and red, respectively. The separation between healthy and ischemic segments is also visualized by the Gaussian distributions on the x-axis for the ground truth and on the y-axis for the ST estimate. A measure of the superposition between the two classes is provided by the AUC in Table I. The AUC of the ground truth is reported in the last column of Table I.

The estimated segmental strain curves on the 4-ch LADdist simulated Toshiba sequence are shown in Fig. 10.

[3]https://gbiomed.kuleuven.be/english/research/50000635/50508167/open-data

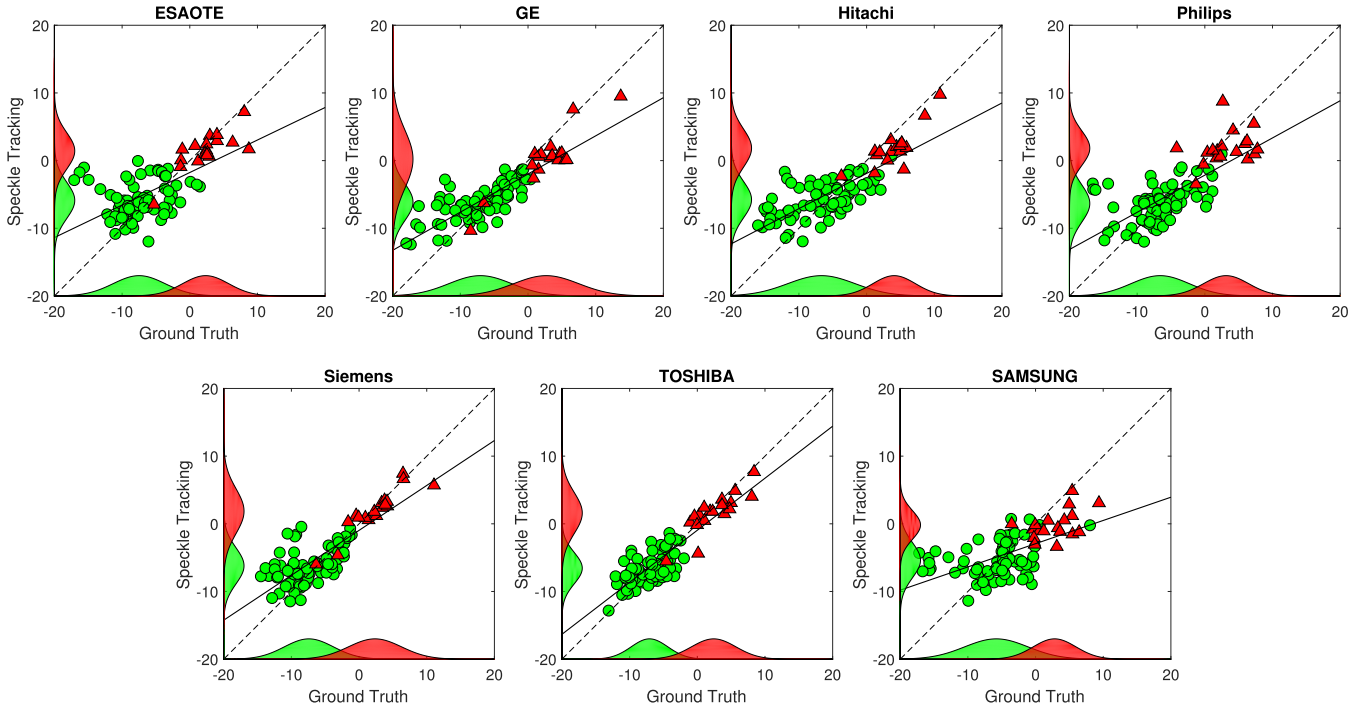

Fig. 9. Correlation plot between ground-truth segmental L-strain (x-axis) and ST estimate (y-axis). Healthy segments are represented as green dots, whereas ischemic segment as red triangles. The Gaussian distributions were computed from the sample mean and standard deviation and provide an intuition of the separation between classes.

TABLE I

RESULTS OF THE CONSIDERED IN-HOUSE ST ALGORITHM, REPORTED SEPARATELY FOR EACH VENDOR SPECIFIC SYNTHETIC DATA SET (FIRST COLUMN). SLOPE OF THE REGRESSION LINE (α), CORRELATION COEFFICIENT (ρ), BIAS (μ), LOAS, AND AUC. ASTERISKS DENOTE STATISTICAL SIGNIFICANCE (REFER TO THE MAIN TEXT FOR ITS DEFINITION)

VENDOR	α	ρ	μ	LOA	AUC	AUC_{GT}
Hitachi	0.52	0.81*	0.30	7.59	0.99*	0.97*
Toshiba	0.77	0.89*	0.29	4.30	0.97*	0.99*
Esaote	0.48	0.60*	1.44	8.06	0.97*	0.98*
Samsung	0.33	0.56*	-0.60	8.87	0.94*	0.96*
Siemens	0.66	0.83*	0.89	5.87	0.96*	0.97*
Philips	0.55	0.73*	-0.02	7.60	0.99*	0.97*
GE	0.56	0.86*	0.29	6.59	0.91*	0.94*

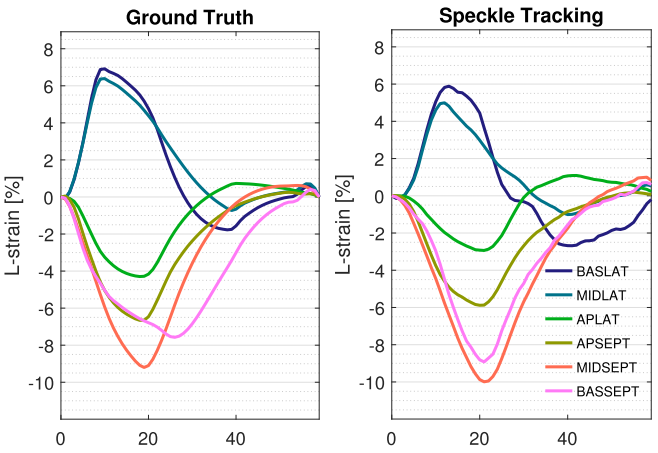

Fig. 10. Segmental L-strain on the synthetic 4-ch LCX Toshiba sequence: (a) Ground truth. (b) In-house ST algorithm.

The estimated profiles follow closely the ground truth and dis-kinetic segments are recovered correctly on this sequence.

V. DISCUSSION

We have presented a pipeline to generate realistic synthetic data for 2-D ST algorithms. The pipeline was used to generate an open-access database of 105 synthetic sequences. The synthetic data sets are diverse in terms of motion pattern, probe orientation, and speckle texture. In particular, we provide image qualities representative of seven different ultrasound systems from different vendors. This was the result of a major logistic effort involving representatives from seven major vendors of ultrasound systems who accepted to provide high-quality template recordings and disclose some of the proprietary acquisition settings especially for this paper. This data set can therefore be used to measure sensitivity to changing global and regional function as well as changing image appearance between vendors.

In terms of mechanical properties, this data set shares some of the limitations of the original pipeline for 3-D simulations [8], [10]. Values of peak systolic longitudinal strain for the healthy case are below reported normality ranges [22]. This is a common limitation of existing heart models and improving this aspect is the topic of ongoing research. Most likely, the low L-strain is due to the absence of the *atrial kick*, in the computational model. Moreover, no postsystolic shortening, which is an important hallmark of ischemia, is present. Finally,

ischemic regions cover full LV segments and are therefore large (see Fig. 3). The sensitivity of STE to the extent of the ischemic region, therefore, cannot be tested at present.

In order to register the 2-D templates with the 3-D model, we assumed a textbook definition of the imaging planes given by known rotations along the LV long axis, as illustrated in Fig. 3. Since template recordings were coming from free-hand scans, there will be therefore an unavoidable mismatch between the real slice position and the assumed one. An error in the 2-D/3-D alignment will affect the sampling of the scatter amplitude (hence, the image texture) and of the deformation field (hence, the ground truth values). In this regard, we note that most of the template recordings were coming from a standardization study [6] in which great care was put in reducing all potential sources of variability coming from data acquisition, such as probe positioning. As such, imaging planes are expected to be as much as possible consistent between vendors and in agreement with standard definitions. Most importantly, in our pipeline, template recordings are "only" used to transfer a realistic visual texture to the simulation. As such, we are not concerned by a small error in the positioning of the slicing plane as far as the visual appearance of the template recording remains plausible.

The usefulness of the multivendor synthetic data set presented here is manifold. On one side, it can be used to guide the development of single-vendor ST solutions. Moreover, it can be used to contrast solutions from different vendors. In this context, we are currently in the process of running a follow up of the initial standardization study [7] where this synthetic data set is being used to benchmark regional strain measurements from nine vendors of STE software packages. This includes the seven manufacturers considered here plus two software only companies. Hereto, it is worth noting that data as provided in the open-access database would not be necessarily readable by commercial systems as several of them use a proprietary data format. Furthermore, the provided data can be used to develop more general ST algorithms not tailored to the images coming from a specific system. Hereto, the availability of realistic synthetic data with associated ground truth displacement could be certainly beneficial in the design of machine-learning based algorithms. Finally, the data set presented here is based on the same set of E/M simulations which were used in [8] to simulate 3-D recordings. The two data sets could therefore be used jointly in order to compare the respective advantages and pitfalls of the 2-D and 3-D ultrasound technology for strain imaging.

We evaluated the feasibility of the provided database as a benchmarking set for ST algorithms by using one recent technique developed in our laboratory. Of note, our goal was not to perform a thorough evaluation of an ST algorithm but rather to show that the synthetic data sets could be tracked and that, therefore, could be used for quality assurance of ST techniques. An in-deep evaluation of ST techniques remains beyond the scope of this paper. The evaluation showed that the data sets could be tracked with reasonable accuracy. In particular, the performance values obtained are in agreement with what reported in a recent comparison study [10]. Yet, [10] was performed on 3-D data and direct comparison is therefore impossible. Of note, we observed a variability in strain accuracy between vendors. Overall, the tested algorithm seemed to perform better on simulated Toshiba images (α closest to 1, highest ρ, low μ, and lowest LOA) and slightly worse on simulated Samsung and ESAOTE images (lowest α, lowest ρ, and largest LOA). This is a direct consequence of the high variability between image appearance from different vendors and shows the difficulty in developing techniques designed to work on generic systems.

We stress that variability in tracking accuracy between vendors is strictly related to our specific ST algorithm and therefore must not be generalized. One source of variability might come from the use of SSD as a data term which, by definition, is intrinsically more sensitive to variations in the changing image appearance between vendors. The use of other feature descriptors more related to image structure, such as mutual information [23] or image phase [24], could reduce such variability. Moreover, it is also important to stress that, although the templates recordings came from commercial systems, all the following steps involved in the generation of the simulated images (scatter map generation, simulation of the RF signals, and image reconstruction) were performed with in-house algorithms. All this can introduce a discrepancy between the appearance of images as produced by a specific system and the respective vendor-specific simulations. Overall, no statement about the superiority of the images of one vendor over another can be made, nor this is the purpose of this paper.

VI. Conclusion

We presented here what to our knowledge is the largest, most realistic, and most diverse ground truth database for 2-D STE algorithms available. The database consists of 105 simulated recordings including: 1) different probe orientations: 2) physiological and pathological contraction patterns: and 3) vendor-specific image quality. The database can be accessed either from our departmental Web page[4] or directly at http://bit.ly/SyntheticDataQA2-DSTE.

Hopefully, this will foster more coordinated and therefore effective and rapid development of the ST technology. This paper responds to a compelling clinical need to reduce inter-vendor variability between clinically available ST solutions.

Acknowledgment

The authors would like to thank Prof. J.-U. Voigt and the EACVI/ASE/Industry Standardization Task Force for providing the high-quality echocardiographic recordings that were used as "templates" in this paper.

References

[1] O. A. Smiseth, H. Torp, A. Opdahl, K. H. Haugaa, and S. Urheim, "Myocardial strain imaging: how useful is it in clinical decision making?" *Eur. Heart J.*, vol. 37, no. 15, pp. 1196–1207, 2015.

[2] K. Kalam, P. Otahal, and T. H. Marwick, "Prognostic implications of global LV dysfunction: A systematic review and meta-analysis of global longitudinal strain and ejection fraction," *Heart*, vol. 100, pp. 1673–1680, 2014.

[3] V. Mor-Avi *et al.*, "Current and evolving echocardiographic techniques for the quantitative evaluation of cardiac mechanics: ASE/EAE consensus statement on methodology and indications endorsed by the Japanese society of echocardiography," *J. Amer. Soc. Echocardiogr.*, vol. 24, no. 3, pp. 277–313, 2011.

[4] J. D. Thomas and L. P. Badano, "EACVI-ASE-industry initiative to standardize deformation imaging: A brief update from the co-chairs," *Eur. Heart J.-Cardiovascular Imag.*, vol. 14, no. 11, p. 1039, 2013.
[5] J.-U. Voigt *et al.*, "Definitions for a common standard for 2D speckle tracking echocardiography: consensus document of the eacvi/ase/industry task force to standardize deformation imaging," *Eur. Heart J.-Cardiovascular Imag.*, vol. 16, no. 1, pp. 1–11, 2014.
[6] K. E. Farsalinos, A. M. Daraban, S. Ünlü, J. D. Thomas, L. P. Badano, and J.-U. Voigt, "Head-to-head comparison of global longitudinal strain measurements among nine different vendors, " *J. Amer. Soc. Echocardiogr.*, vol. 28, no. 10, pp. 1171–1181, 2015.
[7] J. D'hooge *et al.*, "Two-dimensional speckle tracking echocardiography: Standardization efforts based on synthetic ultrasound data," *Eur. Heart J.-Cardiovascular Imag.*, vol. 17, no. 6, pp. 693–701, 2016.
[8] M. Alessandrini *et al.*, "A pipeline for the generation of realistic 3D synthetic echocardiographic sequences: Methodology and open-access database," *IEEE Trans. Med. Imag.*, vol. 34, no. 7, pp. 1436–1451, Jul. 2015.
[9] S. Marchesseau *et al.*, "Preliminary specificity study of the Bestel–Clément–Sorine electromechanical model of the heart using parameter calibration from medical images," *J. Mech. Behavior Biomed. Mater.*, vol. 20, pp. 259–271, Apr. 2013.
[10] M. Alessandrini *et al.*, "Detailed evaluation of five 3D speckle tracking algorithms using synthetic echocardiographic recordings," *IEEE Trans. Med. Imag.*, vol. 35, no. 8, pp. 1915–1926, Aug. 2016.
[11] Y. Zhou *et al.*, "A framework for the generation of realistic synthetic cardiac ultrasound and magnetic resonance imaging sequences from the same virtual patients," *IEEE Trans. Med. Imag.*, to be published.
[12] H. Gao *et al.*, "hooge, "A fast convolution-based methodology to simulate 2-Dd/3-D cardiac ultrasound images," *IEEE Trans. Ultrason., Ferroelect., Freq. Control*, vol. 56, no. 2, pp. 404–409, Feb. 2009.
[13] M. Alessandrini *et al.*, "Generation of ultra-realistic synthetic echocardiographic sequences to facilitate standardization of deformation imaging," in *Proc. IEEE 12th Int. Symp. Biomed. Imag. (ISBI)*, Apr. 2015, pp. 756–759.
[14] B. Heyde *et al.*, "Elastic image registration versus speckle tracking for 2-D myocardial motion estimation: A direct comparison *in vivo*," *IEEE Trans. Med. Imag.*, vol. 32, no. 2, pp. 449–459, Feb. 2013.
[15] Q. Fang and D. Boas, "Tetrahedral mesh generation from volumetric binary and grayscale images," in *Proc. IEEE Int. Symp. Biomed. Imag., From Nano Macro (ISBI)*, Jun./Jul. 2009, pp. 1142–1145.
[16] J. Allard *et al.*, "SOFA—An open source framework for medical simulation," in *Medicine Meets Virtual Reality 15* (Studies in Health Technology and Informatics), vol. 125. 2017, pp. 13–18. [Online]. Available: http://ebooks.iospress.nl/publication/10703
[17] M. D. Cerqueira *et al.*, "Standardized myocardial segmentation and nomenclature for tomographic imaging of the heart: A statement for healthcare professionals from the cardiac imaging committee of the council on clinical cardiology of the american heart association," *Circulation*, vol. 105, no. 4, pp. 539–542, 2002.
[18] A. Myronenko, "Non-rigid image registration regularization, algorithms and applications," Ph.D. dissertation, Oregon Health Sci. Univ., Portland, OR, USA, 2010.
[19] F. L. Bookstein, "Principal warps: Thin-plate splines and the decomposition of deformations," *IEEE Trans. Pattern Anal. Mach. Intell.*, vol. 11, no. 6, pp. 567–585, Jun. 1989.
[20] B. Chakraborty, B. Heyde, M. Alessandrini, and J. D'hooge, "Fast myocardial strain estimation from 3d ultrasound through elastic image registration with analytic regularization," *Proc. SPIE*, vol. 9790, pp. 979006-1–979006-7, Apr. 2016.
[21] E. R. DeLong, D. M. DeLong, and D. L. Clarke-Pearson, "Comparing the areas under two or more correlated receiver operating characteristic curves: A nonparametric approach," *Biometrics*, vol. 44, no. 3, pp. 837–845, 1988.
[22] T. Yingchoncharoen, S. Agarwal, Z. Popović, and T. H. Marwick, "Normal ranges of left ventricular strain: A meta-analysis," *J. Amer. Soc. Echocardiogr.*, vol. 26, no. 2, pp. 185–191, 2012.
[23] D. Mattes, D. R. Haynor, H. Vesselle, T. K. Lewellyn, and W. Eubank, "Nonrigid multimodality image registration," *Proc. SPIE*, vol. 4322, pp. 4322-1–4322-12, Jul. 2001. [Online]. Available: http://dx.doi.org/10.1117/12.431046
[24] M. Alessandrini, H. Liebgott, D. Barbosa, and O. Bernard, "Monogenic phase based optical flow computation for myocardial motion analysis in 3D echocardiography," in *Statistical Atlases and Computational Models of the Heart. Imaging and Modelling Challenges* (Lecture Notes in Computer Science), vol. 7746, O. Camara, T. Mansi, M. Pop, K. Rhode, M. Sermesant, and A. Young, Eds. Berlin, Germany: Springer, 2013, pp. 159–168.

Martino Alessandrini received the Ph.D. degree in information technology from the University of Bologna, Bologna, Italy, in 2011.

He held a post-doctoral position at the CREATIS Laboratory, Lyon, France, from 2011 to 2013, and with the Department of Cardiovascular Sciences, KU Leuven, Leuven, Belgium, from 2013 to 2015. He is currently a Marie Curie Fellow with the Department of Electrical Engineering, University of Bologna. His research aims to a better understanding of diagnosis and treatment of cardiac disease by using complementary techniques including image analysis computational modeling and machine learning. He has co-authored over 60 papers and conference proceedings in this field.

Bidisha Chakraborty received the B.Tech. degree in electronics and communication from Techno India University, Kolkata, India, in 2009, and the M.Sc. degree in information and communication from the Technical University of Hamburg, Hamburg, Germany, in 2013. She is currently pursuing the master's degree with KU Leuven, Leuven, Belgium.

Her current interest is image processing.

Brecht Heyde received the B.Sc. degree in chemical engineering and the M.Sc. degree in biomedical engineering from Ghent University, Ghent, Belgium, in 2007 and 2009, respectively, and the Ph.D. degree from KU Leuven, Leuven, Belgium, in 2013, with a focus on 2-D and 3-D cardiac strain imaging.

He currently holds a postdoctoral research position in the same lab at KU Leuven and was a postdoc at Duke University, Durham, NC, USA, between 2015 and 2016. He is currently with Materialise, where he is working on orthopaedic planning software to manufacture 3-D printed knee guides to facilitate total and partial knee replacement surgeries. He has published and co-authored over 50 scientific papers in international journals and conference proceedings on ultrasound deformation imaging. His current research interests include image registration, beamforming strategies, and high frame rate imaging.

Dr. Heyde was nominated for the Young Investigator Award at the IEEE International Ultrasonics Symposium in 2010. He has been the Chair of the Ultrasound Conference of the SPIE Medical Imaging Symposium since 2015.

Olivier Bernard received the M.Sc. degree in electrical engineering and the Ph.D. degree in medical image processing from the Institut national des sciences appliquées, University of Lyon, Lyon, France, in 2006.

In 2007, he was a Post-Doctoral Research Fellow with the Federal Polytechnic Institute of Lausanne, Lausanne, Switzerland, in the laboratory headed by Prof. M. Unser. In 2007, he became an Associate Professor with the University of Lyon and a member of the CREATIS Laboratory, CNRS 5220, INSERM U1044, INSA-Lyon, University of Lyon. In 2013, he was an Invited Professor with the Federal Polytechnic Institute of Lausanne in the laboratory headed by Prof. J. P. Thiran. His current research interests include medical image analysis with a particular attention to cardiac imaging, image reconstruction, image segmentation, motion analysis, statistical modeling, sampling theories, and machine learning.

Dr. Bernard received the special mention (second prize) for the best Ph.D. in France awarded by the IEEE Engineering in Medicine and Biology Society in 2008. He was an Associate Editor of the IEEE TRANSACTIONS ON IMAGE PROCESSING journal for four years.

Mathieu De Craene received the Ph.D. degree from the Université Catholique de Louvain, Ottignies-Louvain-la-Neuve, Belgium.

He was a Post-Doctoral Researcher with Universitat Pompeu Fabra, Barcelona, Spain, from 2006 to 2012. He joined Philips Research, Suresnes, France, in 2012. He was involved in validating cardiac tracking algorithms by organizing various collaborations between Philips and academic partners. He has been involved in image processing (mainly image registration) for more than ten years, specializing in cardiac deformation image analysis.

Maxime Sermesant received the Diploma degree in general engineering from Ecole Centrale Paris, Châtenay-Malabry, France, in 1999, the M.Sc. degree from École normale Supérieure Paris-Saclay, Cachan, France, in 1999, and the Ph.D. degree in control, signal, and image processing from the University of Nice Sophia Antipolis, Nice, France in 2003.

From 2003 to 2005, he was a Research Fellow with the Cardiac Magnetic Resonance Research Group, Guy's Hospital, King's College London, London, U.K. Since 2005, he has been a Research Scientist with the Asclepios Team, INRIA, Sophia Antipolis, France, and a part-time Lecturer with the Division of Imaging Sciences, St Thomas' Hospital, King's College London. His main focus in recent years has been the application of patient-specific models of the heart to cardiac pathologies. His research interests include biomedical image processing and organ modeling. The integration of these two areas opens up possibilities in clinical data analysis for diagnosis and in pathology simulation for therapy planning.

Jan D'hooge (M'98) received the M.Sc. and Ph.D. degrees in physics from KU Leuven, Leuven, Belgium, in 1994 and 1999, respectively. His dissertation studied the interaction of ultrasonic waves and biological tissues using computer simulation.

As a Post-Doctoral Researcher with the Medical Imaging Computing Laboratory, KU Leuven, he was involved in elastic registration, segmentation, shape analysis, and data acquisition problems related to other modalities (in particular, magnetic resonance imaging). In 2006, he was appointed Associate Professor with the Department of Cardiovascular Diseases of the Medical Faculty. Since 2009, he has been a part-time Visiting Professor with the Norwegian Institute of Science and Technology, Trondheim, Norway. He has (co)-authored over 150 peer-reviewed papers, has contributed to eight books, and has co-edited one book. His current research interests include myocardial tissue characterization, deformation imaging, and cardiac pathophysiology.

Dr. D'hooge received the Young Investigator Award of the Belgian Society of Echocardiography in 1999, and he was nominated for the Young Investigator Award of the European Society of Echocardiography in 2000. He is a member of the Acoustical Society of America and the European Association of Echocardiography. He was the Chair of the Ultrasound Conference of the SPIE Medical Imaging Symposium from 2008 to 2011, the Technical Vice-Chair of the IEEE Ultrasonics Symposium from 2008 to 2012, and the Technical Chair of the IEEE Ultrasonics Symposium in 2014. He was an elected AdCom member of the IEEE UFFC Society from 2010 to 2012.